Kinetic Unfolding Mechanism of the Inducible Nitric Oxide Synthase Oxygenase Domain Determined by Time-Resolved Electrospray Mass Spectrometry†

Derek J. Wilson,‡ Steven P. Rafferty,§ and Lars Konermann*,‡

Department of Chemistry, The University of Western Ontario, London, Ontario N6A 5B7, Canada, and Department of Chemistry, Trent University, Peterborough, Ontario K9J 7B8, Canada

Received October 29, 2004; Revised Manuscript Received December 14, 2004

ABSTRACT: The inducible nitric oxide synthase core oxygen domain ($iNOS_{COD}$) is a homodimeric protein complex of ca. 100 kDa. In this work, the subunit disassembly and unfolding of the protein following a pH jump from 7.5 to 2.8 were monitored by on-line rapid mixing in conjunction with electrospray (ESI) time-of-flight mass spectrometry. Various protein species become populated during the denaturation process. These can be distinguished by their ligand binding behavior, and by the different charge states that they produce during ESI. Detailed intensity−time profiles were obtained for all of these species, and the kinetics were subjected to a global analysis which allows a model of the denaturation process to be developed. The data are described well by three relaxation times ($\tau_1 = 0.36$ s, $\tau_2 = 0.62$ s, and $\tau_3 = 3.3$ s), each of which has a characteristic amplitude spectrum. The initial step of the reaction is the disruption of the $iNOS_{COD}$ dimer, to generate heme-bound monomeric species in various degrees of unfolding. This first step is accompanied by the loss of two tetrahydrobiopterin cofactors. Subsequent heme loss generates monomeric apoproteins exhibiting various degrees of unfolding. In addition, the formation of proteins that are bound to two heme groups is observed. A subpopulation of holo monomers undergoes substantial unfolding while retaining contact with the heme cofactor. Together with previous studies, the results of this work suggest that the occurrence of complex reaction mechanisms involving several short-lived intermediates is a common feature for the denaturation of large multiprotein complexes.

Nitric oxide (NO)[1] is involved in numerous physiological processes, including cell signaling and host defense (*1*). In mammals, NO is produced by the nitric oxide synthase (NOS) family of enzymes. One member of this family, inducible NOS (iNOS), is typically expressed in response to inflammatory mediators (*2*−*4*). All NOS enzymes are active only as homodimers, and catalyze the oxidation of arginine to NO and citrulline, using NADPH and molecular oxygen as cosubstrates (*3*). Each of the two ∼130−160 kDa enzyme subunits exhibits a modular structure, comprising an N-terminal oxygenase domain, a calmodulin binding site, and a C-terminal reductase domain. The core region of the oxygenase domain ($iNOS_{COD}$, residues 76−500 in mouse iNOS) forms the active site where NO synthesis takes place. This core region binds heme, tetrahydrobiopterin (H_4B), and arginine, and it also is the site of dimerization (*2*).

The modular organization of the NOS enzymes offers the possibility of studying the properties of individual domains separately. For example, isolated $iNOS_{COD}$ dimerizes and binds its cofactors (*5*). Upon dimerization, mobile hydrophobic regions of the monomers fold and sequester two molecules of H_4B at the dimer interface in the vicinity of the heme cofactors (*6*). The pentacoordinate heme iron is bound to the proximal Cys194 via a cytochrome P450-like thiolate ligation. The factors governing the dimerization process are not well understood, but it appears that heme insertion and formation of the metal−thiolate bond are critical steps that allow the formation of subunit interactions to proceed (*4*, *7*). A specific disruption of iNOS dimerization has been the target of several pharmacologic studies aimed at treating chronic inflammation caused by overexpression of the enzyme (*8*−*11*). It appears that work in this area could benefit from a better general understanding of the iNOS assembly and disassembly processes.

Electrospray ionization mass spectrometry (ESI-MS) is a particularly powerful approach for studying noncovalent protein complexes. It provides direct information about the subunit stoichiometry, and it allows the binding of cofactors to be monitored (*12*−*15*). In addition, ESI-MS can distinguish solution-phase conformations of proteins, based on the number of protons acquired during the ESI process. A protein in a tightly folded conformation will generate lower protonation states than the same protein in a more unfolded conformation (*16*). A number of studies strongly suggest that

† This work was supported by the Natural Sciences and Engineering Research Council of Canada (NSERC), the Canada Foundation for Innovation (CFI), The Province of Ontario, and the Canada Research Chairs Program.

* To whom correspondence should be addressed. Telephone: (519) 661-2111, ext 86313. Fax: (519) 661-3022. E-mail: konerman@uwo.ca.

‡ The University of Western Ontario.

§ Trent University.

[1] Abbreviations: $iNOS_{COD}$, inducible nitric oxide synthase core oxygenase domain; DTT, dithiothreitol; ESI, electrospray ionization; MS, mass spectrometry; H_4B, tetrahydrobiopterin; NO, nitric oxide; NOS, nitric oxide synthase; NADP, nicotinamide adenine dinucleotide phosphate.

10.1021/bi047684y CCC: $30.25
Published on Web 01/29/2005

each conformational state in solution gives rise to a bell-shaped ESI charge state envelope (*17*, *18*). Recently, Smith et al. (*19*) used ESI-MS for studying quaternary interactions, cofactor binding, and protein conformation in $iNOS_{COD}$ as a function of pH under equilibrium conditions. In near-neutral solutions, the intact $iNOS_{COD}$ dimer was observed together with tightly folded heme-bound monomers. Heme-bound monomers in semi-unfolded conformations were the dominant species at pH 3.5. Further acidification induced unfolding of these monomers, along with loss of the heme (*19*).

A thorough characterization of protein unfolding processes requires equilibrium experiments to be complemented by kinetic studies. For many years, it was assumed that kinetic intermediates do not become populated during protein unfolding because of their low stability under strongly denaturing conditions (*20*). However, computer simulations indicate that complex energy landscapes with multiple barriers are a commonplace occurrence not only for folding but also for the unfolding of proteins (*21*, *22*). This view has been confirmed in several studies on small monomeric proteins, which have provided direct experimental evidence for the formation of kinetic intermediates during denaturation (*23*, *24*). Recent work has also confirmed the existence of kinetic intermediates for larger systems, such as hemoglobin (*25*) and GroEL (*26*). Despite these advances, many of the general principles guiding the subunit disassembly and unfolding processes of multiprotein complexes remain to be uncovered.

In this work, time-resolved ESI-MS is employed to investigate the denaturation of $iNOS_{COD}$ following a pH jump. The experiments make use of a recently developed ESI-coupled capillary mixing system (*27*, *28*) that is employed in conjunction with a time-of-flight mass analyzer. This setup allows ESI mass spectra to be measured at specific reaction times, and it provides detailed intensity−time profiles of individual conformational species and ligand-binding states. It is shown that the $iNOS_{COD}$ unfolding process involves several transient intermediates. Despite its greater overall complexity, the kinetics follow a general progression similar to that observed under equilibrium conditions.

EXPERIMENTAL PROCEDURES

Materials. Mouse $iNOS_{COD}$ was expressed in LE392-(λDE3) *Escherichia coli* cells that were transformed with a pET23 (His_6 tag) plasmid as described previously (*29*). The His_6 tag does not seem to have an impact on either the conformation or the dimerization properties of the protein (*29*). Purified $iNOS_{COD}$ in 10 mM sodium phosphate buffer (pH 7.5) was flash-frozen in liquid nitrogen and stored at −20 °C. Prior to use, aliquots of the stock solution were dialyzed overnight at 4 °C against 10 mM ammonium acetate solution (Fluka, Buchs, Switzerland) containing 7 μM H_4B (Sigma, St. Louis, MO) and 100 μM DTT (Sigma) at pH 7.5. Arginine, which had originally been present during protein preparation, was lost during this dialysis step. Arginine removal was necessary because measurements under solution conditions designed to maintain the presence of this cosubstrate resulted in kinetic data with a poor signal-to-noise ratio. Protein concentrations were determined on the basis of an ϵ_{396} of 74 mM^{-1} cm^{-1} for the monomeric holoprotein.

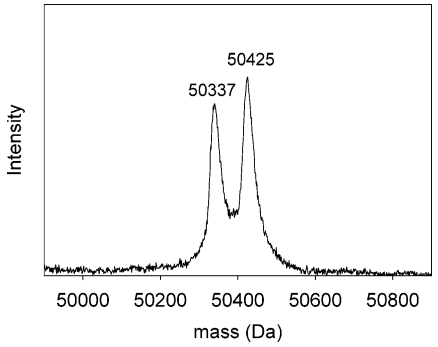

FIGURE 1: Deconvoluted ESI mass distribution of monomeric apo-$iNOS_{COD}$, indicating the presence of two components with different masses. These forms of the protein will be termed "light" (50 337 Da) and "heavy" (50 425 Da).

$iNOS_{COD}$ Primary Structure. On the basis of the amino acid sequence, including the His_6 tag, the expected mass of the apo-$iNOS_{COD}$ monomer is 50 548.6 Da. The deconvoluted ESI mass spectrum of the apoprotein (obtained after acidification to pH 2.8, Figure 1) shows two peaks of roughly equal intensity, corresponding to masses of 50 425 and 50 337 Da. It seems likely that this phenomenon is related to N-terminal truncation (*19*). An acceptable match with the two measured masses is obtained by postulating that both forms of the protein carry an 80 Da covalent adduct. The two peaks could then be ascribed to loss of Met-Ala (50 346 Da + 80 Da = 50 426 Da) and to loss of Met-Ala-Ser (50 259 Da + 80 Da = 50 339 Da), respectively. A mass shift of 80 Da could be caused by phosphorylation. iNOS has previously been observed to take up stoichiometric quantities of phosphate (*30*), but phosphorylated proteins are not commonly produced from bacterial hosts. A thorough investigation of the factors underlying the observed peak splitting is beyond the scope of this work and will be addressed in a future study. It is noted that this heterogeneity has little relevance for the experiments discussed here, as both forms of the protein appear to be kinetically indistinguishable.

Time-Resolved ESI-MS. Kinetic ESI-MS experiments were carried out using a capillary mixing setup with an adjustable reaction chamber volume. A detailed description of the device is given in ref *28*. Briefly, this continuous-flow apparatus consists of two concentric capillaries, each of which is connected to a syringe to allow for infusion of two reactant solutions. The two solutions are mixed at the end of the inner (fused silica) capillary, and the reaction is allowed to proceed until pneumatically assisted ESI occurs at the outlet of the outer (stainless steel) capillary. The reaction time is controlled by the flow rates from the syringes, and by the volume between the mixing point and the outer capillary outlet. Mass spectra can be recorded for selected reaction times by acquiring data with the mixer held at specific positions. To acquire kinetic data (i.e., intensity−time profiles), the inner capillary is withdrawn continuously such that time-dependent changes in signal intensity can be observed for all ions in the mass spectrum. For this work, this setup was adapted to allow the coupling to an LCT time-of-flight mass spectrometer (Micromass). For unfolding experiments, $iNOS_{COD}$ [30 μM in 10 mM ammonium acetate (pH 7.5)] and acetic acid [10% (v/v) in 10 mM ammonium acetate] were each infused at a rate of 20 μL/min for a total

flow rate of 40 μL/min and a final pH of 2.8. To facilitate the detection of large noncovalent complexes, the mass spectrometer was operated by using high-pressure conditions in the ion transfer region (*31*, *32*). For $iNOS_{COD}$, a source pressure of 10 mbar, with sample cone and extraction cone voltages of 90 and 5 V, respectively, proved to be optimal for obtaining kinetic data. The relative intensity of highly charged protein ions (in the range of *m*/*z* 1000−3000) could be increased by using even lower extraction cone potentials (data not shown). Consistent with earlier studies, this observation shows that the appearance of ESI mass spectra can strongly depend on the instrument conditions that are used (*33*). However, for a given set of voltage parameters, the spectra obtained were highly reproducible. All data were collected using the MassLynx instrument software. Time-dependent ion intensities were extracted and baseline-corrected from the total ion count profiles as described previously (*25*). In the case of split peaks (see the previous paragraph), kinetic profiles were obtained from the lighter of two species to minimize interference due to peak tailing. Additionally, a correction was made to account for the distortion of the time axis due to laminar-flow effects (*28*).

Global Data Analysis. The data analysis strategy used centers on the idea that protein folding and unfolding can be described in terms of coupled first-order differential equations (*34*). Thus, time-dependent mass spectral signals for any *m*/*z*, $I(m/z,t)$, can be expressed as a linear combination of exponential expressions (*25*, *35*, *36*).

$$I(m/z,t) = \sum_{j=1}^{n-1} C_j(m/z) \exp(-t/\tau_j) + C_n(m/z) \qquad (1)$$

The $n - 1$ relaxation times, τ_j, are common to all signal−time profiles across the entire *m*/*z* range, and the observed kinetics differ only in the amplitudes $C_j(m/z)$. The kinetic behavior of each relaxation component *j* can be visualized by plotting its amplitude spectrum, i.e., by displaying the C_j values as a function of *m*/*z*. Positive amplitudes correspond to decay processes or lag phases, whereas negative amplitudes reflect an intensity increase. $C_n(m/z)$ is the amplitude spectrum of the nondecaying component, representing the extrapolated ESI mass spectrum for $t = \infty$. The relative error of the fitted relaxation times can be obtained by using an exhaustive search strategy (*37*). It was found to be on the order of 10%.

RESULTS AND DISCUSSION

ESI-MS of Native $iNOS_{COD}$. Figure 2 shows an ESI mass spectrum of $iNOS_{COD}$ recorded at pH 7.5 and at a solution flow rate of 10 μL/min. It is dominated by ions corresponding to the intact dimer, but also shows some monomeric species. This spectrum is very similar to data obtained previously by nano-ESI-MS (*19*). Identification of the ion composition is slightly complicated by the fact that it is common for large proteins and protein complexes to be poorly desolvated, which increases the mass of the observed ions, and induces peak broadening (*38*, *39*). In addition, the sample contains two types of protein chains with slightly different masses, as shown in Figure 1. With these factors in mind, the observed dimer mass is compatible with the assumption of a complex containing two heme groups (2 × 616.2 Da) and two molecules of H_4B (2 × 241.1 Da), as shown in the top inset of Figure 2. The dimer peaks show a low mass shoulder that is tentatively assigned to ions which have lost both H_4B cofactors, possibly due to the occurrence of a gas-phase dissociation process (*40*). The monomer peaks appear as doublets, corresponding to ions with and without heme (bottom inset in Figure 2). The mass observed for these monomeric species does not allow for the presence of H_4B. This is consistent with the fact that H_4B binding occurs at the monomer−monomer interface of the complex such that the binding site is disrupted upon dissociation of the dimer. Close inspection of Figure 2 also reveals the presence of monomeric heme-free and heme-bound ions in the range of *m*/*z* 1000−3000. These highly charged species are attributed to the presence of a minor population of more unfolded proteins in solution. Overall, the data in Figure 2 are consistent with the notion that $iNOS_{COD}$ at pH 7.5 predominantly exists as a dimeric complex containing two heme groups and two molecules of H_4B.

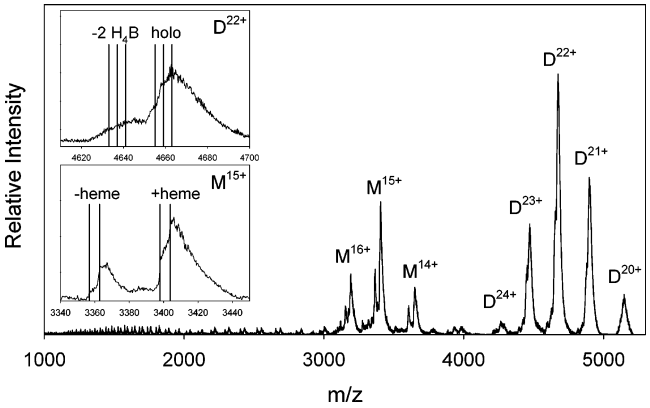

FIGURE 2: ESI mass spectrum of $iNOS_{COD}$ obtained under native conditions [10 mM ammonium acetate (pH 7.5)]. The peaks are identified as monomer (M) or dimer (D) ions with the charge state indicated. (Top inset) Close-up view of the +22 dimer signal. The triplet of lines labeled holo corresponds to the masses expected for dimers representing the light−light, light−heavy, and heavy−heavy monomer combinations (see the legend of Figure 1). These expected dimer masses assume the presence of two heme groups, and two molecules of H_4B. The triplet on the left indicates the masses expected for dimers after loss of the two H_4B moieties. (Bottom inset) Close-up view of the +15 monomer peak. The line doublets labeled +heme and −heme correspond to the masses of the two monomer types with and without heme, respectively, in the absence of H_4B.

Time-Resolved Mass Spectra. For the kinetic experiments described in this work, the denaturation of $iNOS_{COD}$ was initiated by exposing the protein to dilute acetic acid, resulting in a pH jump from 7.5 to 2.8. ESI mass spectra recorded at selected reaction times are shown in Figure 3. The earliest time point that could be studied corresponds to a reaction time of ∼9 ms (Figure 3A). Compared to the data obtained at pH 7.5 (Figure 2), this spectrum shows an increase in the relative intensities of monomer ions, and a concomitant decrease in the relative dimer intensities. In addition, there is a general shift to lower charge states, with the dimer maximum shifting from +22 to +20, and the monomer maximum shifting from +15 to +14. It cannot be ruled out that these spectral changes are partially due to the occurrence of burst-phase phenomena, i.e., very rapid changes in the protein structure in solution. It seems very

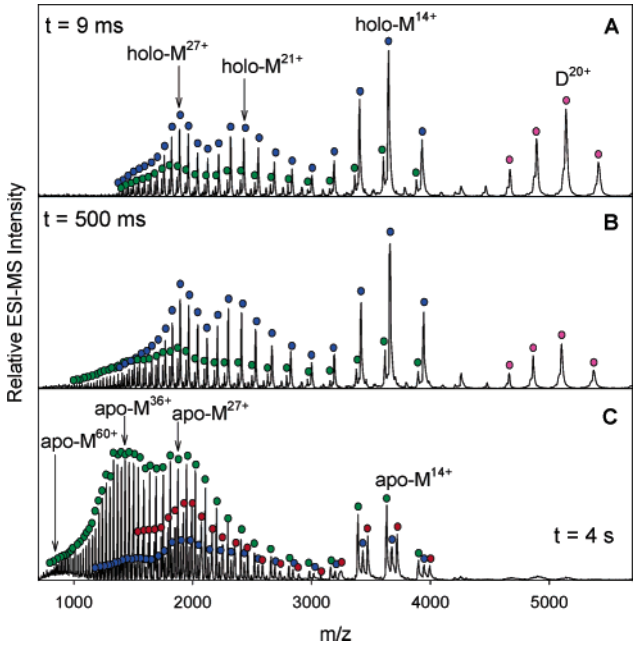

FIGURE 3: Time-resolved ESI mass spectra of $iNOS_{COD}$, recorded at different times following a pH jump from 7.5 to 2.8: (A) $t \sim 9$ ms, (B) $t = 500$ ms, and (C) $t = 4$ s. Ions corresponding to the intact $iNOS_{COD}$ dimer, with two heme groups and two molecules of H_4B bound, are denoted with a D (marked with magenta circles). Heme-bound monomers are denoted holo-M (blue symbols). apo-M represents monomeric proteins that are not bound to any cofactor (green symbols). Monomeric proteins that carry two heme groups are marked with red circles. Also indicated are the charge states of some of the protein ions. The data were obtained by operating the rapid-mixing setup in "spectral mode" (*28*), i.e., by recording spectra for selected (fixed) distances between the mixer and ESI source.

likely, however, that a major portion of the observed spectral alterations is due to the different ESI conditions used for the kinetic experiments. A general trend toward charge reduction has been observed previously in protein solutions containing acetic acid. This effect has been attributed to gas-phase processes, and it does not indicate the occurrence of solution-phase conformational changes (*41*, *42*). Control experiments indicate that the higher solution flow rate used in Figure 3A (60 μL/min, vs 10 μL/min in Figure 2) is partially responsible for the increase in the relative intensity of monomeric protein ions. It is noted that "secondary" effects of this kind complicate the interpretation of spectral changes only in cases where the ESI conditions are altered, such as for Figures 2 and 3A. Once the pH jump has occurred, however, the ESI conditions remain constant for the rest of the experiment. Therefore, the differences between the three ESI mass spectra depicted in Figure 3 can be directly attributed to changes in the $iNOS_{COD}$ conformation or ligand-binding state in solution.

A reaction time of 500 ms (Figure 3B) marks the point at which the relative intensities of heme-bound monomers are highest. Interestingly, these ions show a trimodal charge state distribution, thus indicating the presence of at least three solution-phase structures. The first group of these peaks, centered around +14, is attributed to heme-bound monomers in a relatively tightly folded conformation. The other two distributions, with maxima around +21 and +27, represent more unfolded species. The transient population of significantly unfolded proteins that remain bound to a heme cofactor is not unprecedented; a similar behavior has previously been observed for hemoglobin (*25*) and myoglobin (*23*). At a reaction time of 4 s (Figure 3C), the $iNOS_{COD}$ dimer has become almost unobservable. Instead, the spectrum is dominated by apo monomers in high charge states, extending up to at least +60. Charge states in this range were not observed for apo monomers formed early during the reaction (Figure 3A). This indicates that the reaction mixture for $t = 4$ s contains apo monomers that are significantly more unfolded than for early time points. However, there remains a distinct group of apo monomer ions, centered around +14, that represents heme-free proteins in a relatively compact solution-phase conformation. Close inspection of Figure 3C also reveals the presence of heme-bound monomer ions (blue circles), which extend their charge state distribution up to +45 and higher.

Another interesting feature observed in the spectrum (Figure 3C) are $iNOS_{COD}$ monomers that carry two heme groups. Similar species were observed in the equilibrium unfolding experiments performed by Smith et al. (*19*). We attribute the formation of these complexes to the tendency of heme to form dimers and higher-order aggregates in solution (*43*). The observation of double-heme species indicates that $iNOS_{COD}$ is capable of binding to a heme dimer. This interpretation is in line with the well-known fact that cofactor binding sites are often highly flexible, thus allowing proteins to interact with numerous different ligands (*44*). In particular, the binding of heme dimers to proteins such as myoglobin has been documented previously by NMR (*45*) and in ESI-MS studies (*46*, *47*). Similarly, it has been shown that flavodoxin binds not only its native FMN cofactor but also an FMN dimer (*48*). The observation of a two-heme species under the conditions of this work is, therefore, not entirely surprising.

No major changes in the ESI mass spectrum of $iNOS_{COD}$ were observed for reaction times longer than 4 s (data not shown). The spectra obtained for times of several minutes show slightly lower intensities for heme-bound monomer ions in charge states +13 to +15, but they are otherwise very similar to the data depicted in Figure 3C. The presence of these monomer ions for long reaction times suggests that a small equilibrium population of compact proteins persists at pH 2.8.

Kinetic Profiles. The experimental approach used in this work provides not only ESI mass spectra for selected reaction times (Figure 3) but also intensity−time profiles for all observable ionic species. Thus, the $iNOS_{COD}$ denaturation kinetics can be visualized in three-dimensional diagrams, where ESI-MS intensities are plotted as a function of m/z and reaction time. On the basis of the different quaternary structures and ligand-binding states of the protein, the kinetic data can be grouped into four categories (Figure 4). All $iNOS_{COD}$ dimer profiles show a rapid decay, reaching intensities close to zero for a reaction time of ~4 s (Figure 4A). A more complex behavior is observed for heme-bound monomers (Figure 4B). Throughout the charge state range from +13 to ca. +35, these ions show kinetics that are typical for a transient intermediate, i.e., a rapid increase that is followed by a slow decay. In contrast, heme-bound monomers in higher charge states show a steady increase toward a maximum value, thus signifying the behavior of a reaction

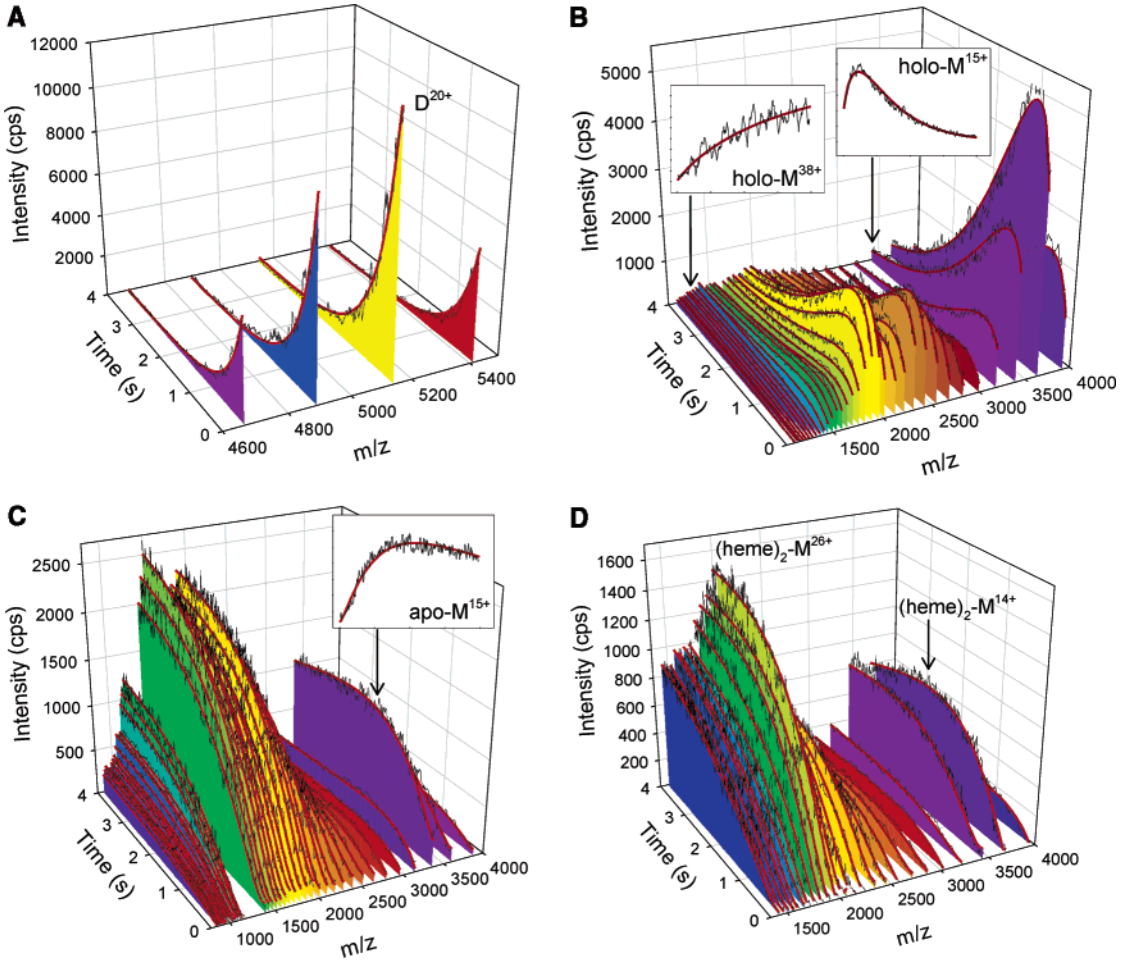

FIGURE 4: Intensity−time profiles for the ionic species that are observed during the acid-induced unfolding of $iNOS_{COD}$: (A) $iNOS_{COD}$ dimer, (B) heme-bound monomer, (C) apo monomer, and (D) monomer carrying two heme groups. Experimental data are displayed as black lines; dark red curves with colored drop planes are multiexponential fits obtained by global analysis. Selected profiles in panels B and C are displayed separately to highlight the kinetic behavior of the underlying solution-phase species. The gap in panel C is due to the overlap of apo monomers and two-heme monomers, which prevents a kinetic analysis of the corresponding ions in the range around *m*/*z* 1400. The data were obtained by operating the rapid-mixing setup in "kinetic mode" (*28*), i.e., by continuously monitoring ion intensities across the entire *m*/*z* range, while continuously increasing the distance between the mixer and ESI source.

product. Figure 4C shows data obtained for apo monomers, which represent the dominant product of the $iNOS_{COD}$ denaturation process. Almost all of the curves in Figure 4C represent highly charged ions that show an intensity increase and level off as they approach a reaction time of 4 s. The occurrence of a lag phase early during denaturation gives these profiles a sigmoidal appearance. Interestingly, the three lowest charge states, +13 to +15, exhibit a different behavior. These profiles carry the signature of a reaction intermediate, i.e., an increase followed by a decrease (Figure 4C inset). The maximum intensity for these curves is reached for a reaction time of ca. 2 s, whereas the holo monomer traces in Figure 4B reach their maxima much earlier, at ~0.5 s. Clearly, this different behavior indicates that the two types of intensity profiles represent different kinetic processes. Figure 4D displays the ESI-MS profiles for $iNOS_{COD}$ ions carrying two heme groups. By and large, these profiles mirror the kinetic behavior displayed for apo monomers in Figure 4C.

Global Analysis of the Kinetic Data. The data displayed in Figure 4 were subjected to a global kinetic analysis. As outlined in Experimental Procedures, the basic premise underlying this procedure is that all the observed spectral changes can be described by a common set of relaxation times, each of which has its characteristic amplitude spectrum. According to eq 1, positive amplitudes correspond to decaying signal intensities or to a lag phase, whereas negative amplitudes represent an intensity increase. It was found that the measured $iNOS_{COD}$ denaturation kinetics were described well by three relaxation times. The fits obtained from the global analysis procedure are shown as red lines superimposed on the experimental data in Figure 4.

The amplitude spectrum of the shortest relaxation time ($\tau_1 = 0.36$ s) is depicted in Figure 5A. The most prominent features of this spectrum are large positive amplitudes for dimer ions (pink), accompanied by negative amplitudes for the heme-bound monomeric protein (blue). This kinetic signature represents the initial step of the denaturation process, namely, the disintegration of the intact $iNOS_{COD}$ dimer (with two heme groups and two H_4B moieties attached) into heme-bound monomers. Both H_4B cofactors are lost during this step. In addition, Figure 5A shows positive amplitudes for apo monomeric species (green) and for monomers carrying two heme groups (red). These amplitudes reflect a delay in the formation of the respective species,

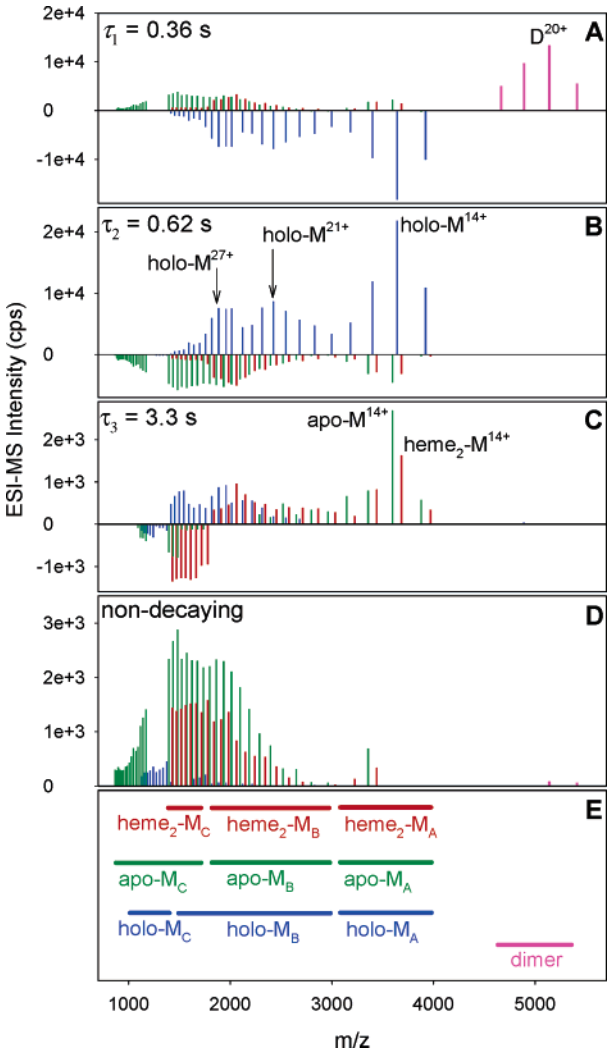

FIGURE 5: Amplitude spectra of the three relaxation times: τ_1 = 0.36 s (A), τ_2 = 0.62 s (B), and τ_3 = 3.3 s (C). Panel D shows the amplitude spectrum of the nondecaying component. The color coding is the same as in Figure 3: magenta for the intact $iNOS_{COD}$ dimer, blue for the heme-bound monomer, green for the apo monomer, and red for monomers bound to two heme groups. Also indicated are the charge states for some of the peaks. Panel E gives the *m*/*z* ranges assigned to the various species involved in the proposed kinetic mechanism (see Figure 6). Subscripts A−C denote an increasing degree of unfolding.

which indicates that they are not a direct product of the dimer dissociation process.

The second relaxation time (τ_2 = 0.62 s) has positive amplitudes for all the heme-bound monomer peaks, representing a decay of the corresponding solution-phase proteins. The accompanying negative amplitudes for the apo monomer ions are shifted to notably higher charge states, which shows that heme loss on the time scale of τ_2 preferentially produces apo monomers in unfolded conformations. Along with these species, monomers that are bound to two heme groups are formed (red negative amplitudes in Figure 5B).

The amplitude spectrum for the τ_3 of 3.3 s is depicted in Figure 5C. Apo monomers and monomers bound to two heme groups show positive amplitudes at low charge states and negative amplitudes at high charge states. This behavior reports on a slow unfolding transition of the two underlying solution-phase species that occurs without a change in the heme binding state. A similar transition is observed for holo monomers, with the exception that the decay process affects only ions below *m*/*z* 3000. It seems possible that the processes associated with τ_3 are related to proline isomerization events, which have previously been shown to cause slow relaxation phenomena during unfolding (*49*, *50*). Figure 5D shows the spectrum of the nondecaying component. As expected, it is similar to the experimental ESI mass spectrum for t = 4 s in Figure 3C.

Proposed Mechanism of $iNOS_{COD}$ Denaturation. Figure 6 shows a proposed kinetic scheme for the denaturation of $iNOS_{COD}$ under acidic conditions. This mechanism is derived from the amplitude spectra discussed in the preceding section. The representation of all kinetic transitions as irreversible events is clearly an oversimplification, because most forms of the protein can still be observed to some degree under equilibrium conditions at pH 2.8. The kinetic data imply that each of the three heme binding states can exist in at least three different solution-phase conformations that are distinguishable on the basis of their ESI charge states. The degree of unfolding is indicated by a subscript, where A represents relatively compact structures, B corresponds to more expanded conformations, and C represents highly unfolded proteins. The assignment of the 3 × 3 monomeric species to specific *m*/*z* regions is indicated in Figure 5E.

The initial step in Figure 6 is the dissociation of the dimer, occurring concomitantly with the loss of H_4B. This process is associated with the amplitude spectrum of τ_1 in Figure 5A. During this step, two kinetically distinct types of heme-bound monomers, holo-M_A and holo-M_B, are generated. The bimodal appearance of the holo-M_B charge state distribution indicates that this kinetic species comprises proteins in at least two conformations. For reasons of simplicity, however, these conformations are denoted as a single species in Figure 6. Holo-M_B is involved in a transition to an even more unfolded monomeric heme-bound species, holo-M_C, on the time scale of τ_3. The occurrence of this process is evident from the positive−negative crossing of the blue amplitude spectrum in Figure 5C. This behavior reflects the kinetic differences between holo monomers in low and high charge states that are highlighted by the two insets in Figure 4B.

The kinetics observed for apo-M_A, apo-M_B, heme$_2$-M_A, and heme$_2$-M_B are virtually identical, indicating the existence of a rapid equilibrium between these solution-phase species (*51*, *52*). The same is true for apo-M_C and heme$_2$-M_C. In Figure 6, the occurrence of these rapid equilibria has been indicated by arranging the two groups of protein species together in boxes. Both holo-M_A and holo-M_B undergo a decay process on the time scale of τ_2 that is associated with changes in the heme binding state. Figure 6 suggests that holo-M_A feeds into the pool containing apo-M_A. Similarly, holo-M_B decays to form apo-M_C and heme$_2$-M_C. This scenario is consistent with the amplitude spectrum of τ_2 in Figure 5B. Finally, the positive−negative transitions of the green and the red spectra in Figure 5C indicate a slow unfolding of apo-M_A, apo-M_B, heme$_2$-M_A, and heme$_2$-M_A. This process occurs on the time scale of τ_3, and it feeds into the pool of apo-M_C and heme$_2$-M_C.

CONCLUSIONS

This work demonstrates that the combination of on-line rapid mixing with ESI time-of-flight mass spectrometry holds

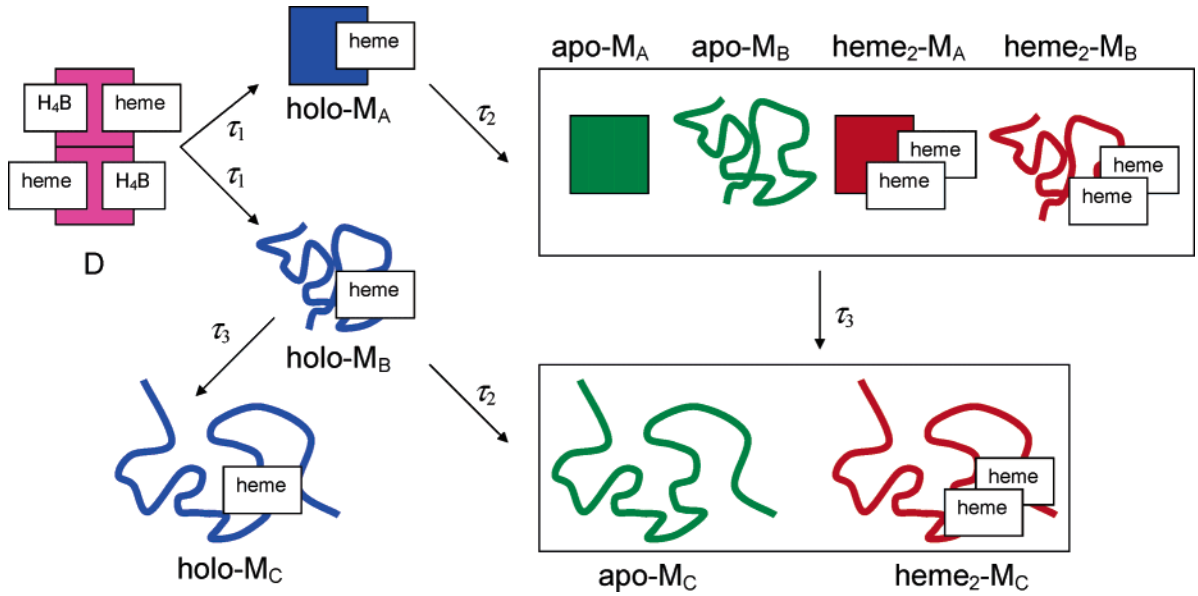

FIGURE 6: Proposed kinetic mechanism for the acid-induced dissociation and unfolding of iNOS$_{COD}$, based on the global analysis results depicted in Figure 5. Boxes indicate groups of species that exhibit the same kinetic behavior. The color coding of individual species is consistent with that used in Figures 3 and 5. Further explanations are given in the text.

considerable potential for studying kinetic processes involving large noncovalent protein complexes. In particular, the ability to identify and monitor coexisting species in multicomponent mixtures is an advantage compared to other time-resolved methods. In this case, the acid-induced denaturation of iNOS$_{COD}$ was shown to follow a complex reaction mechanism. It was found that several intermediates are involved in this process, namely, two types of heme-bound monomers, apo monomers exhibiting various degrees of unfolding and proteins carrying two heme groups. The kinetic data were dissected by using a global analysis approach such that the observed ESI-MS intensity changes could be assigned to specific relaxation times. Thus, it could be determined that the denaturation of iNOS$_{COD}$ follows a mechanism that involves parallel unfolding pathways. When considered in the context of previous kinetic unfolding studies on hemoglobin (*25*) and GroEL (*26*), the results of this work suggest that the occurrence of complex reaction mechanisms involving several short-lived intermediates is a common feature for the denaturation of large multiprotein complexes. As in the case of hemoglobin (*25*), the overall kinetic unfolding mechanism of iNOS$_{COD}$ resembles that observed under equilibrium conditions, but shows a higher degree of complexity (*19*).

It appears that experimental approaches similar to those employed here have great potential for studies on the assembly, dynamics, and function of large biomolecular complexes. Additional insights into the structure of short-lived intermediates could be provided by using on-line rapid mixing and ESI-MS in conjunction with covalent labeling techniques or isotope exchange methods.

ACKNOWLEDGMENT

We thank Jeffrey C. Smith for providing protein samples, Doug Hairsine for expert support with operation of the LCT mass spectrometer, and Douglas A. Simmons for helpful discussions.

REFERENCES

1. Ignarro, L. J. (1999) Nitric Oxide: A Unique Endogenous Signaling Molecule in Vascular Biology (Nobel Lecture), *Angew. Chem., Int. Ed. 38*, 1882−1892.
2. Stuehr, D. J. (1999) Mammalian Nitric Oxide Synthases, *Biochim. Biophys. Acta 1411*, 217−230.
3. Andrew, P. J., and Mayer, B. (1999) Enzymatic Function of Nitric Oxide Synthases, *Cardiovasc. Res. 43*, 521−531.
4. Alderton, W. K., Cooper, C. E., and Knowles, R. G. (2001) Nitric Oxide Synthases: Structure Function and Inhibition, *Biochem. J. 357*, 593−615.
5. Ghosh, D. K., and Stuehr, D. J. (1995) Macrophage NO Synthase: Characterization of Isolated Oxygenase and Reductase Domains Reveals a Head-to-Head Subunit Interaction, *Biochemistry 34*, 801−807.
6. Crane, B. R., Arvai, A. S., Ghosh, D. K., Wu, C., Getzoff, E. D., Stuehr, D. J., and Tainer, J. A. (1998) Structure of Nitric Oxide Synthase Oxygenase Dimer with Pterin and Substrate, *Science 279*, 2121−2126.
7. Wilson, D. J., and Rafferty, S. P. (2001) A Sturctural Role for Tryptophan 188 of Inducible Nitric Oxide Synthase, *Biochem. Biophys. Res. Commun. 287*, 126−129.
8. Panda, K., Rosenfeld, R., Ghosh, S., Meade, A. L., Getzoff, E. D., and Stuehr, D. J. (2002) Distinct Dimer Interaction and Regulation in Nitric Oxide Synthase Types I, II, and III, *J. Biol. Chem. 277*, 31020−31030.
9. Blasko, E., Glaser, C. B., Devlin, J. J., Xia, W., Feldman, R. I., Polokoff, M. A., Phillips, G. B., Whitlow, M., Auld, D. S., McMillan, K., Ghosh, S., Stuehr, D. J., and Parkinson, J. F. (2002) Mechanistic Studies with Potent and Selective Inducible Nitric Oxide Synthase Dimerization Inhibitors, *J. Biol. Chem. 277*, 295−302.
10. Sennequier, N., Wolan, D., and Stuehr, D. J. (1999) Antifungal Imidazoles Block Assembly of Inducible NO Synthase into an Active Dimer, *J. Biol. Chem. 274*, 930−938.
11. Ratovitski, E. A., Bao, C., Quick, R. A., McMillan, A., Kozlovsky, C., and Lowenstein, C. J. (1999) An Inducible Nitric Oxide Synthase (NOS)-Associated Protein Inhibits NOS Dimerization and Activity, *J. Biol. Chem. 274*, 30250−30257.
12. Loo, J. A. (2000) Electrospray Ionization Mass Spectrometry: A Technology for Studying Noncovalent Macromolecular Complexes, *Int. J. Mass Spectrom. 200*, 175−186.
13. Heck, A. J. R., and Van den Heuvel, R. H. H. (2004) Investigation of intact protein complexes by mass spectrometry, *Mass Spectrom. Rev. 23*, 368−389.
14. Potier, N., Donald, L. J., Chernushevich, I., Ayed, A., Ens, W., Arrowsmith, C. H., Standing, K. G., and Duckworth, H. W. (1998) Study of a noncovalent trp repressor:DNA operator complex by

electrospray ionization time-of-flight mass spectrometry, *Protein Sci. 7*, 1388−1395.
15. McCammon, M. G., and Robinson, C. V. (2004) Structural change in response to ligand binding, *Curr. Opin. Chem. Biol. 8*, 60−65.
16. Chowdhury, S. K., Katta, V., and Chait, B. T. (1990) Probing Conformational Changes in Proteins by Mass Spectrometry, *J. Am. Chem. Soc. 112*, 9012−9013.
17. Kaltashov, I. A., and Eyles, S. J. (2002) Studies of Biomolecular Conformations and Conformational Dynamics by Mass Spectrometry, *Mass Spectrom. Rev. 21*, 37−71.
18. Grandori, R. (2002) Detecting equilibrium cytochrome *c* folding intermediates by electrospray ionization mass spectrometry: Two partially folded forms populate the molten globule state, *Protein Sci. 11*, 453−458.
19. Smith, J. C., Siu, M. K. W., and Rafferty, S. P. (2004) Collisional Cooling Enhances the Ability to Observe Non-Covalent Interactions Within the Inducible Nitric Oxide Synthase Oxygenase Domain: Dimerization, Complexation and Dissociation, *J. Am. Soc. Mass Spectrom. 15*, 629−638.
20. Juneja, J., and Udgaonkar, J. B. (2002) Characterization of the Unfolding of Ribonuclease A by a Pulsed Hydrogen Exchange Study: Evidence for Competing Pathways for Unfolding, *Biochemistry 41*, 2641−2654.
21. Lazaridis, T., and Karplus, M. (1997) "New View" of Protein Folding Reconciled with the Old Through Multiple Unfolding Simulations, *Science 278*, 1928−1931.
22. Chan, H. S., and Dill, K. A. (1998) Protein Folding in the Landscape Perspective: Chevron Plots and Non-Arrhenius Kinetics, *Proteins: Struct., Funct., Genet. 30*, 2−33.
23. Sogbein, O. O., Simmons, D. A., and Konermann, L. (2000) The Effects of pH on the Kinetic Reaction Mechanism of Myoglobin Unfolding Studied by Time-Resolved Electrospray Ionization Mass Spectrometry, *J. Am. Soc. Mass Spectrom. 11*, 312−319.
24. Sridevi, K., and Udgaonkar, J. B. (2003) Surface Expansion Is Independent of and Occurs Faster than Core Solvation during the Unfolding of Barstar, *Biochemistry 42*, 1551−1563.
25. Simmons, D. A., Wilson, D. J., Lajoie, G. A., Doherty-Kirby, A., and Konermann, L. (2004) Subunit Disassembly and Unfolding Kinetics of Hemoglobin Studied by Time-resolved Electrospray Mass Spectrometry, *Biochemistry 43*, 14792−14801.
26. Chen, J., and Smith, D. L. (2000) Unfolding and Disassembly of the Chaperonin GroEL Occurrs via a Tetradecameric Intermediate with a Folded Equatorial Domain, *Biochemistry 39*, 4250−4258.
27. Wilson, D. J., and Konermann, L. (2004) Mechanistic Studies on Enzymatic Reactions by Electrospray Ionization MS Using a Capillary Mixer with Adjustable Reaction Chamber Volume for Time-Resolved Measurements, *Anal. Chem. 76*, 2537−2543.
28. Wilson, D. J., and Konermann, L. (2003) A Capillary Mixer With Adjustable Reaction Chamber Volume for Millisecond Time-Resolved Studies by Electrospray Mass Spectrometry, *Anal. Chem. 75*, 6408−6414.
29. Rafferty, S. P., Boyington, J. C., Kulansky, R., Sun, P. D., and Malech, H. L. (1999) Stoichiometric Arginine Binding to the Oxygenase Domain of Inducible Nitric Oxide Synthase Requires a Single Molecule of Tetrahydrobiopterin per Dimer, *Biochem. Biophys. Res. Commun. 257*, 344−347.
30. Nathan, C., and Xie, Q. (1994) Regulation of Biosynthesis of Nitric Oxide, *J. Biol. Chem. 269*, 13725−13728.
31. Tahallah, N., Pinkse, M., Maier, C. S., and Heck, A. J. R. (2001) The effect of the source pressure on the abundance of ions of noncovalent protein assemblies in an electrospray ionization orthogonal time-of-flight instrument, *Rapid Commun. Mass Spectrom. 15*, 596−601.
32. Chernushevich, I. V., and Thomson, B. A. (2004) Collisional cooling of large ions in electrospray mass spectrometry, *Anal. Chem. 76*, 1754−1760.
33. Vaidyanathan, S., Kell, D. B., and Goodacre, R. (2004) Selective Detection of Proteins in Mixtures Using Electrospray Ionization Mass Spectrometry: Influence of Instrumental Settings and Implications for Proteomics, *Anal. Chem. 76*, 5024−5032.
34. Pain, R. H. (2000) *Mechanisms of Protein Folding*, 2nd ed., Oxford University Press, New York.
35. Beechem, J. M., Ameloot, M., and Brand, L. (1985) Global and Target Analysis of Complex Decay Phenomena, *Anal. Instrum. 14*, 379−402.
36. Holzwarth, A. R. (1995) Time-Resolved Fluorescence Spectroscopy, *Methods Enzymol. 246*, 334−362.
37. Konermann, L., Collings, B. A., and Douglas, D. J. (1997) Cytochrome *c* Folding Kinetics Studied by Time-Resolved Electrospray Ionization Mass Spectrometry, *Biochemistry 36*, 5554−5559.
38. Green, B. N., and Vinogradov, S. N. (2004) An Electrospray Ionization Mass Spectrometric Study of the Subunit Structure of the Giant Hemoglobin from the Leech *Nephelopsis oscura*, *J. Am. Soc. Mass Spectrom. 15*, 22−27.
39. Griffith, W. P., and Kaltashov, I. A. (2003) Highly asymmetric interactions between globin chains during hemoglobin assembly revealed by electrospray ionization mass spectrometry, *Biochemistry 42*, 10024−10033.
40. Collings, B. A., and Douglas, D. J. (1996) Conformation of Gas-Phase Myoglobin Ions, *J. Am. Chem. Soc. 118*, 4488−4489.
41. Mirza, U. A., and Chait, B. T. (1994) Effects of Anions on the Positive Ion Electrospray Ionization Mass Spectra of Peptides and Proteins, *Anal. Chem. 66*, 2898−2904.
42. Konermann, L., and Douglas, D. J. (1998) Equilibrium Unfolding of Proteins Monitored by Electrospray Ionization Mass Spectrometry: Distinguishing Two-State from Multi-State Transitions, *Rapid Commun. Mass Spectrom. 12*, 435−442.
43. Adams, P. A. (1976) The Kinetics and Mechanism of the Recombination Reaction between Apomyoglobin and Haemin, *Biochem. J. 159*, 371−376.
44. Davis, A. M., and Teague, S. J. (1999) Hydrogen Bonding, Hydrophobic Interactions, and Failure of the Rigid Receptor Hypothesis, *Angew. Chem., Int. Ed. 38*, 736−749.
45. Deeb, R. S., and Peyton, D. H. (1992) Proton NMR Study of the Interaction of Tin(IV) Protoporphyrin IX Monomers and Dimers with Apomyoglobin, *Biochemistry 31*, 468−474.
46. Lee, V. W. S., Chen, Y.-L., and Konermann, L. (1999) Reconstitution of Acid-Denatured Holo-Myoglobin Studied by Time-Resolved Electrospray Ionization Mass Spectrometry, *Anal. Chem. 71*, 4154−4159.
47. Simmons, D. A., and Konermann, L. (2002) Characterization of Transient Protein Folding Intermediates During Myoglobin Reconstitution by Time-Resolved Electrospray Mass Spectrometry with On-Line Isotopic Pulse Labeling, *Biochemistry 41*, 1906−1914.
48. Muralidhara, B. K., and Wittung-Stafshede, P. (2003) Can Cofactor-Binding Sites in Proteins be Flexible? *Desulfovibrio desulfuricans* Flavodoxin Binds FMN Dimer, *Biochemistry 42*, 13074−13080.
49. Brandts, J. F., Halvorson, H. R., and Brennan, M. (1975) Consideration of the Possibility That the Slow Step in Protein Denaturation Reactions Is Due to Cis−Trans Isomerism of Proline Residues, *Biochemistry 14*, 4953−4963.
50. Kiefhaber, T., Quaas, R., Hahn, U., and Schmid, F. X. (1990) Folding of Ribonuclease T1. 1. Existence of Multiple Unfolded States Created by Proline Isomerisation, *Biochemistry 29*, 3053−3061.
51. Wagner, D. S., and Anderegg, R. J. (1994) Conformation of Cytochrome *c* Studied by Deuterium Exchange-Electrospray Ionization Mass Spectrometry, *Anal. Chem. 66*, 706−711.
52. Simmons, D. A., Dunn, S. D., and Konermann, L. (2003) Conformational Dynamics of Partially Denatured Myoglobin Studied by Time-Resolved Electrospray Mass Spectrometry With Online Hydrogen−Deuterium Exchange, *Biochemistry 42*, 5896−5905.

BI047684Y